Neural Control of Voluntary Movement Initiation

Doug P. Hanes and Jeffrey D. Schall*

When humans respond to sensory stimulation, their reaction times tend to be long and variable relative to neural transduction and transmission times. The neural processes responsible for the duration and variability of reaction times are not understood. Single-cell recordings in a motor area of the cerebral cortex in behaving rhesus monkeys (*Macaca mulatta*) were used to evaluate two alternative mathematical models of the processes that underlie reaction times. Movements were initiated if and only if the neural activity reached a specific and constant threshold activation level. Stochastic variability in the rate at which neural activity grew toward that threshold resulted in the distribution of reaction times. This finding elucidates a specific link between motor behavior and activation of neurons in the cerebral cortex.

A major goal of cognitive neuroscience is to develop linking propositions—statements that explain behavior and the associated mental processes in terms of brain function. Since Helmholtz's demonstration (*1*) that behavioral reaction times, which measure the duration of mental processes, were long and variable rather than instantaneous, experimental psychologists have characterized reaction times and developed sophisticated models of possible underlying processes. Concurrently, neuroscientists have identified brain circuits that are involved in movement generation (*2*, *3*). However, few studies have integrated both paradigms to directly investigate mechanisms that regulate initiation of voluntary movements. It seems clear that a simple summation of sensory and motor transduction delays and conduction times in the nervous system cannot account for the duration and variability of reaction times. Evidently, decision processes intervene.

Mathematical models of the decision and response preparation processes that lead to movement initiation have been proposed. One general class of models, known as accumulator models, seems most amenable to physiological evaluation. In accumulator models, a response is triggered when a signal that represents the decision process, which is referred to as the activation function, grows over time to reach a threshold level. Different sources responsible for the duration and variability of reaction times have been proposed by two alternative models: a variable rate model (*4*) and a variable threshold model (*5*) (Fig. 1). Although both models have been used to describe performance in reaction-time tasks, neurophysiological approaches that test and refine such models are essential for understanding the neural basis of movement initiation.

We compared the physiological merits of the variable rate and variable threshold models of reaction time in macaques by monitoring the activity of single cells in the frontal eye field (FEF), an area in the frontal cortex that plays a central role in production of voluntary eye movements (*6*). This investigation focused on the activity of neurons that exhibit increased activity specifically related to saccade production (*3*, *7*). For each recording session, we positioned a microelectrode in the FEF of a rhesus monkey (*Macaca mulatta*) (*8*). For each neuron, the range of saccades associated with the largest activation, the movement field, was determined by presenting a saccade target at different locations. Monkeys then performed a countermanding task that manipulates the ability to inhibit a movement at different stages of preparation (Fig. 2) (*9*). We analyzed the growth of movement-related activity of FEF neurons during trials with different reaction times to test the merits of the two models (*10*). To represent the form of the accumulating signal, we derived a particular activation function from the trains of action potentials (*11*).

We recorded from two *M. mulatta* a total of 118 cells, 25 of which exhibited movement-related activity and provided sufficient data in the necessary trial conditions to be included in this report. The response of a representative FEF movement cell is shown during 150 no-signal trials when the saccade target was in the movement field of the cell (Fig. 3A). The activity of the cell began to increase ~100 ms before saccade initiation and peaked shortly after saccade initiation.

Specific measures of movement-related neural activity were required to evaluate the predictions of the two models. The first prediction involved whether the trigger threshold varied with reaction time. We tested this prediction by measuring the level of the neural activation function at the

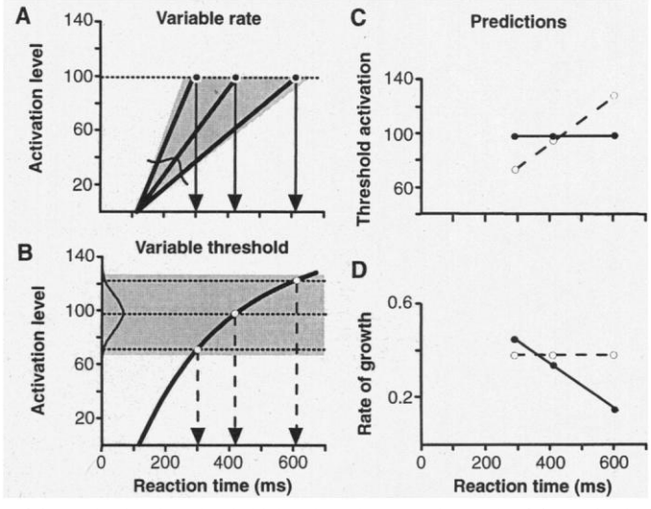

Fig. 1. Schematic representations of the variable rate and variable threshold models of reaction time. Thick solid lines represent the activation functions; dotted lines represent the movement trigger activation thresholds. In the variable rate model (**A**), the trigger activation threshold does not vary across trials; instead, the rate of growth of the activation function varies in a Gaussian fashion across trials as indicated by the Gaussian distribution on the activation functions. Short reaction times occur when the rate of growth of the activation function is high; when the rate of growth of the activation function is low, longer reaction times occur. The activation function for this model is a linear function of time. The characteristic long tail of the reaction time distributions arises from the relation of the slope of the linear activation function to the constant threshold. In the variable threshold model (**B**), the activation function does not vary, but the movement trigger threshold varies across trials in a Gaussian fashion, as indicated by the Gaussian distribution on the ordinate. Short reaction times occur when the trigger threshold activation is low; as the threshold activation increases, longer reaction times occur. The activation function for this model is a decelerating exponential function; a function of this form is needed in this model to generate the skewed reaction-time distributions. The form of the predicted threshold activation levels (**C**) and rates of growth of the activation function (**D**) as a function of reaction times are shown for the variable rate (solid circles, solid line) and the variable threshold (open circles, dashed line) models. The three points plot the values indicated by arrows in (A) and (B).

Department of Psychology, Wilson Hall, Vanderbilt University, Nashville, TN 37240, USA.

*To whom correspondence should be addressed. E-mail: schalljd@ctrvax.vanderbilt.edu

time the presumed threshold that triggers the movement was crossed. On the basis of electrophysiological studies of the FEF, we estimate that measurements of neural activity 10 to 20 ms before saccade initiation are an accurate index of the level of trigger threshold activation (*12*). We defined the threshold activation as the average level of the activation function 10 to 20 ms before movement initiation. We compared the threshold activation across groups of no-signal trials with different reaction times. The activity of the representative FEF movement cell in trials with shorter and longer reaction times is shown in Fig. 3, B and C. The threshold activation for the group of trials with short reaction times (99 spikes/s) was essentially the same as the threshold activation for the group of trials with long reaction times (97 spikes/s). To increase the statistical power of the analysis, we divided the trials (Fig. 3A) into 10 reaction time groups (Fig. 3D) (*13*). The threshold activation for these 10 groups of trials ranged from 91 to 105 spikes/s with an average (±SEM) of 97 ± 3.0 spikes/s. A linear regression analysis indicated no relation between the threshold activation and reaction time ($P > 0.05$) for this cell. No change in threshold activation with reaction time was observed in 23 of 25 cells. This result is consistent with the variable rate but not the variable threshold model.

The second prediction of both models involved the rate of growth of the activation function. To determine whether the rate of growth of activity varied with reaction time, it was necessary to identify when the activation function began to grow, which we accomplished by a Poisson spike train analysis (*14*). A linear regression was then fit to the activation function from the defined onset of activity to 15 ms before saccade initiation. The rate of growth of the movement-related activity, that is, the acceleration of action potential production, was defined as the slope of the least squares best-fit line. For the activation functions, the slopes of the best-fit lines were 1.4 spikes/s^2 (coefficient of determination r^2 = 0.98) and 0.64 spikes/s^2 (r^2 = 0.97), respectively (Fig. 3, B and C). The rate of growth of the activation function is plotted against reaction time (Fig. 3E) for the 10 reaction time groups shown in Fig. 3D. The rates of growth ranged from 1.8 to 0.6 spikes/s^2 (minimum r^2 = 0.87, maximum r^2 = 0.99) with an average of 1.25 ± 0.10 spikes/s^2 (*15*). A linear regression analysis indicated that the rate of growth of the activation function for this cell decreased significantly with increasing reaction time [$F(9) = 24.42$, $P < 0.01$]. In 22 of 25 cells, the rate of growth of the activation function declined significantly with increasing reaction time ($P < 0.01$). This result is consistent with the variable rate but not the variable threshold model.

The countermanding task provides an experimental test of the validity of the constant trigger threshold attribute of the variable rate model. If a critical trigger threshold activation must be crossed to initiate a movement, then the level of activity measured in successfully inhibited trials, that is, signal-inhibit trials, should not exceed the threshold activation level measured during no-signal trials, because a saccade was not initiated. To undertake this analysis, it is necessary to obtain a measure of neural activation in signal-inhibit trials to com-

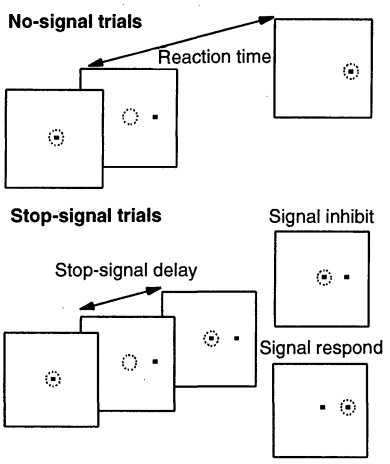

Fig. 2. Countermanding task. Dotted circle indicates the focus of gaze. All trials began with the presentation of a central fixation spot. After fixation of this spot for a variable interval (250 to 350 ms), a target appeared at one of two locations, either in the movement field of the cell or in the opposite hemifield. Simultaneously, the fixation spot disappeared, signaling the monkey to generate a saccade to the target. On 25%, 33%, or 50% of the trials after a delay, referred to as the stop-signal delay, the fixation spot reappeared, instructing the monkey to inhibit movement initiation. During the trials in which the stop signal was not presented (no-signal trials), monkeys were rewarded for generating a single saccade to the peripheral target within 700 ms. During stop-signal trials, monkeys were rewarded for maintaining fixation on the central spot for 700 ms (signal-inhibit trials). If the monkeys did generate a saccade to the peripheral target (signal-respond trials), no reward was given. Four stop-signal delays were used so that, at the shortest stop-signal delay, monkeys inhibited the movement in more than 85% of the stop-signal trials; at the longest delay, monkeys inhibited the movement in fewer than 15% of the stop-signal trials.

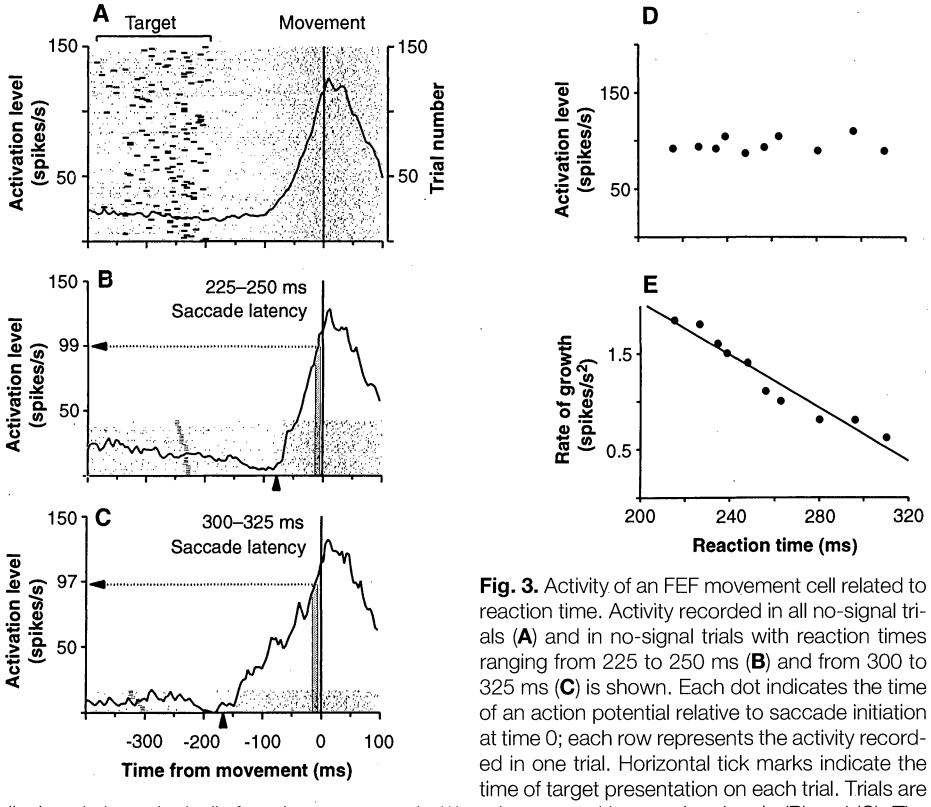

Fig. 3. Activity of an FEF movement cell related to reaction time. Activity recorded in all no-signal trials (**A**) and in no-signal trials with reaction times ranging from 225 to 250 ms (**B**) and from 300 to 325 ms (**C**) is shown. Each dot indicates the time of an action potential relative to saccade initiation at time 0; each row represents the activity recorded in one trial. Horizontal tick marks indicate the time of target presentation on each trial. Trials are displayed chronologically from bottom to top in (A) and are sorted by reaction time in (B) and (C). The average activation function for each group of trials is plotted as a solid line. Dotted arrows in (B) and (C) indicate the average level of activation in the 10- to 20-ms interval before saccade initiation (shaded region). (**D**) Average activation level 10 to 20 ms before saccade initiation is plotted against mean reaction time for 10 reaction time groups for this cell. (**E**) The rate of growth of the activation function for the same 10 reaction time bins is shown. The statistically significant linear regression is indicated.

pare with the threshold activation measured in no-signal trials. However, by definition, neural activity could not be measured with respect to a movement in signal-inhibit trials. The most conservative alternative was to measure the peak neural activation in signal-inhibit trials. Thus, the maximum level of activity that occurred in each signal-inhibit trial was identified during an interval delimited by the shortest and the longest no-signal reaction times obtained for that cell. Then the average neural activation was measured in a 10-ms interval extending from 5 ms before to 5 ms after the peak. A ratio was calculated for each cell by dividing the average peak activation level during signal-inhibit trials by the threshold activation during no-signal trials. In 19 of 25 cells, the neural activity in trials when monkeys withheld a movement was significantly less likely to reach the trigger threshold level than in trials when the monkey executed the movement (t test, $P < 0.05$, minimum ratio = 0.40, maximum ratio = 1.40, mode = 0.75, mean = 0.80). This result is a necessary condition for the constant threshold attribute of the variable rate model and is consistent with event-related potentials recorded in humans (*16*).

An important test of the variable rate model is to determine whether the quantitative variation in the rate of growth of the physiologically measured activation functions could account for the range of reaction times generated by the monkeys. The distribution of the behavioral reaction times collected while recording from each individual FEF cell was compared with a distribution of reaction times generated by a computer simulation run with parameters derived from the activity of that cell. The parameters used for each simulation of a linear accumulator with a constant threshold were derived from the average threshold activation level and the rates of growth of premovement activation obtained from each neuron individually (*17*). A distribution of simulated reaction times was generated to compare with the behavioral reaction times measured while recording from each cell. The simulated distribution of reaction times was often indistinguishable from the observed distribution of reaction times (Fig. 4A). Overall, the simulated reaction time density function based on the physiological data from 9 of 22 cells did not differ in shape or central tendency from the reaction time density function generated by the monkeys (χ^2 test, $P > 0.05$). The distribution of reaction times generated by the monkeys while we were recording from many cells was multimodal, possibly because of the limited number of trials (<50). In these cases, the shapes but not the mean values of the simulated and observed reaction time density functions were different (χ^2 test, $P < 0.05$) (Fig. 4B). Overall, the means of the simulated reaction times were not different from the means of the reaction times generated by the monkey during our collection of data from 17 of 22 cells. Excluding one outlier 17.2 SD from the grand mean, we found the average difference between the means of the simulated reaction times and the means of the observed reaction times was 1.5 ± 1.8 ms, which was not different from 0 [$t(20) = 0.96$]. Thus, by using parameters derived directly from measures of the activity of individual neurons, we could predict the distributions of the reaction times generated by the monkey in these experimental conditions.

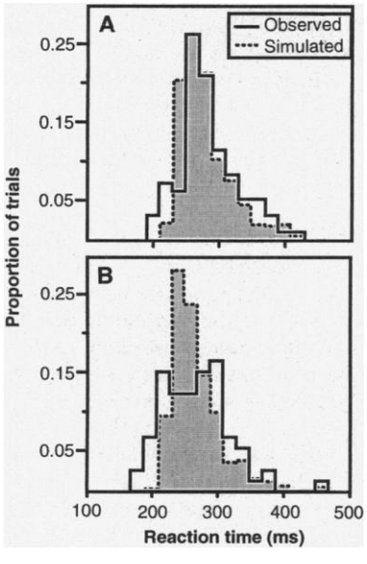

Fig. 4. Probability densities of 95 (**A**) and 47 (**B**) observed reaction times while recording from two FEF cells with movement-related activity (open bins, solid lines) on which are superimposed 5000 simulated reaction times (shaded bins, dotted lines).

This work demonstrates that the irreducible variability of the timing of voluntary movements is a consequence of a particular form of stochastic variability in neural circuits. We speculate that dysfunctional growth of movement-related activity may be a basis for the impaired control of action associated with neurologic and mental disorders. Further work is needed to determine whether, before each movement, the growth of activation is correlated within and across the numerous cortical and subcortical centers involved in movement production. Also, continued efforts combining psychology and neuroscience hopefully will provide insight into whether the random variability of neural activity responsible for producing movements is unpreventable biological noise or a desirable adaptation necessary for flexible behavior.

REFERENCES AND NOTES

1. H. L. F. von Helmholtz, *Philos. Mag.* (English translation) **6**, 313 (1853); R. D. Luce, *Response Times: Their Role in Inferring Elementary Mental Organization* (Oxford Univ. Press, New York, 1986); D. E. Meyer, A. M. Osman, D. E. Irwin, S. Yantis, *Biol. Psychol.* **26**, 3 (1988).
2. V. B. Brooks, *The Neural Basis of Motor Control* (Oxford Univ. Press, New York, 1986).
3. R. H. Wurtz and M. E. Goldberg, *The Neurobiology of Saccadic Eye Movements* (Elsevier, New York, 1989); R. H. S. Carpenter, *Eye Movements* (Macmillan, London, 1991); J. D. Schall, in *Vision and Visual Dysfunction*, vol. 4 of *The Neural Basis of Visual Function*, A. G. Leventhal, Ed. (Macmillan, London, 1991), pp. 388–442.
4. R. H. S. Carpenter, *Movements of the Eyes* (Pion, London, 1988); R. Ratcliff, *Psychol. Rev.* **85**, 59 (1978); J. L. McClelland, *ibid.* **86**, 287 (1979); R. H. S. Carpenter and M. L. L. Williams, *Nature* **377**, 59 (1995).
5. G. R. Grice, *Psychol. Rev.* **75**, 359 (1968); T. A. Nazir and A. M. Jacobs, *ibid.* **53**, 281 (1991). Hybrid models have also been formulated [A. Pacut, *Biol. Cyber.* **28**, 63 (1977)].
6. Several lines of evidence document the role of the FEF, located in the rostral bank of the arcuate sulcus in monkeys, in gaze control (*3*). The FEF projects heavily to subcortical oculomotor structures. Microstimulation with very low current evokes eye movements, and acute inactivation prevents monkeys from making eye movements [E. C. Dias, M. Kiesau, M. A. Segraves, *J. Neurophysiol.* **74**, 2744 (1995)].
7. D. P. Hanes, K. G. Thompson, J. D. Schall, *Exp. Brain Res.* **103**, 85 (1995).
8. Physiological recording techniques have been described (*7*). Monkeys were seated within a magnetic field to monitor eye position by means of a scleral search coil. Experiments were under computer control (PDP 11/83) to present stimuli, deliver a juice reward, and sample and store eye position (250 Hz) and unit activity (1000 Hz). Visual stimuli were presented on a color video monitor (47° by 60°). Animals were cared for in accordance with the National Institutes of Health Guide for the Care and Use of Laboratory Animals and the guidelines of the Vanderbilt Animal Care and Use Committee.
9. G. D. Logan and W. B. Cowan, *Psychol. Rev.* **91**, 295 (1984); D. P. Hanes and J. D. Schall, *Visual Neurosci.* **12**, 929 (1995).
10. Movement-related activity was distinguished from visually evoked activity by a memory-guided saccade task. In this task, the target was flashed for 100 ms while the monkey was required to maintain fixation on the central spot for another 500 to 1000 ms. When the fixation spot disappeared, reward was contingent on the monkey making a saccade to the remembered location of the target. Once the saccade was made, the target reappeared to provide feedback and a target for the monkey to fixate.
11. Activation functions were generated by convolving the spike trains with a function that resembled a postsynaptic potential: $A(t) = [1 - \exp(-t/\tau_g)][\exp(-t/\tau_d)]$, where activation level as a function of time [$A(t)$] varies according to τ_g, the time constant for the growth phase, and τ_d, the time constant for the decay phase. Physiological data from excitatory synapses indicate that $\tau_g \approx 1$ ms and $\tau_d \approx 20$ ms [R. J. Sayer, M. J. Friedlander, S. J. Redman, *J. Neurosci.* **10**, 826 (1990)]. This asymmetric function that represents the actual postsynaptic influence of each cell has two advantages. First, each spike exerts influence only forward in time. Second, time constants that are comparable with physiologically measured values were used.
12. Several physiological findings delimit the interval during which FEF activity could contribute to the commitment to produce a saccadic eye movement. Om-

nipause neurons in the brainstem, which gate saccade initiation, cease discharging 8 to 10 ms before saccade initiation [J. A. Buttner-Ennever, B. Cohen, M. Pause, W. Fries, *J. Comp. Neurol.* **267**, 307 (1988)], and the transduction time from FEF movement cells to the omnipause cells is around 4 ms [M. A. Segraves, *J. Neurophysiol.* **68**, 1967 (1992)]. According to these times, then, the FEF cannot influence saccade initiation later than 12 to 14 ms before the movement begins. Also, the modal time of burst onset within FEF movement cells is 10 ms before saccade initiation (*7*). Finally, the minimum latency of the saccades evoked by electrical stimulation of FEF is around 20 ms [C. J. Bruce, M. E. Goldberg, C. Bushnell, G. B. Stanton, *J. Neurophysiol.* **54**, 714 (1985)]. The results of the analysis we report did not change when the level of activation was measured 20 to 30 or 0 to 10 ms before saccade initiation.

13. All trials for a neuron were rank ordered by reaction time and were split into equal groups containing at least 10 trials on the basis of reaction time. Thus, the first group consisted of the trials with the 10 shortest reaction times, and so on. The number of reaction-time groups varied across cells because of different trial numbers. If the total number of no-signal trials was less than 50, the number of trials in each saccade latency group was set so that five saccade latency groups were generated.
14. An algorithm was applied to each trial to identify periods of activity in which more spikes occurred than would be predicted from a random Poisson process having the overall average rate of the trial [C. R. Legéndy and M. Salcman, *J. Neurophysiol.* **53**, 926 (1985); (*7*)]. For each group of reaction time trials, the mode of the distribution of response beginning times was determined.
15. There were a total of 190 saccade latency groups across all 25 cells. The average r^2 of the linear regression on the activation function was 0.79 (minimum = 0.34, maximum = 0.99). A Durbin-Watson test for autocorrelation of the residuals provided another test of the goodness of fit of the neural activation function with a line. For only 12 of the 190 saccade latency groups was there a significant autocorrelation between the residuals. The fact that a linear function provided such a good fit to the activation function is further evidence against the variable threshold model that posits a decelerating accumulator function.
16. The magnitude of the lateralized readiness potential at movement initiation does not vary with reaction time [G. Gratton, M. G. H. Coles, E. Sirevaag, C. W. Eriksen, E. Donchin, *J. Exp. Psychol. Human Percept. Perform.* **14**, 331 (1988)], and the lateralized readiness potential does not reach a critical threshold level in signal-inhibit trials [R. DeJong, M. G. H. Coles, G. D. Logan, G. Gratton, *ibid.* **16**, 164 (1990)].
17. The reaction time on the *i*th simulation trial was $RT_i = t_{ON} + (A'/r_i)$, where t_{ON} is the onset latency of the cell, A' is the threshold activation level, and r is the rate of growth of the activation function. The onset latency of the growth of the accumulator (t_{ON}), specified by the Poisson spike-train analysis, was held constant across simulated trials. The trigger threshold (A') was held constant across simulated trials at the average threshold activation measured across all reaction time groups collected for that cell (for example, Fig. 3D). The rate of growth of the simulated accumulator function (r) was selected on each simulated trial from a Gaussian distribution. The mean and SD of the sampled Gaussian distribution were derived from the rates of growth of the activation functions across the reaction-time groups collected for that cell (for example, Fig. 3E).
18. We thank O. Armstrong and D. King for assistance with data acquisition and analysis and N. Bichot, R. Blake, R. Carpenter, K. Cave, J. Kaas, J. Lappin, and K. Thompson for helpful discussion and comments on the manuscript. Supported by National Institute of Mental Health grants F31-MH11178 to D.P.H. and R01-MH55806 to J.D.S. and National Eye Institute (of NIH) grant P30-EY08126 to the Vanderbilt Vision Research Center. J.D.S. is a Kennedy Center Investigator.

2 July 1996; accepted 23 August 1996

Preferential Formation of Benzo[*a*]pyrene Adducts at Lung Cancer Mutational Hotspots in *P53*

Mikhail F. Denissenko, Annie Pao, Moon-shong Tang,* Gerd P. Pfeifer*

Cigarette smoke carcinogens such as benzo[*a*]pyrene are implicated in the development of lung cancer. The distribution of benzo[*a*]pyrene diol epoxide (BPDE) adducts along exons of the *P53* gene in BPDE-treated HeLa cells and bronchial epithelial cells was mapped at nucleotide resolution. Strong and selective adduct formation occurred at guanine positions in codons 157, 248, and 273. These same positions are the major mutational hotspots in human lung cancers. Thus, targeted adduct formation rather than phenotypic selection appears to shape the *P53* mutational spectrum in lung cancer. These results provide a direct etiological link between a defined chemical carcinogen and human cancer.

Lung cancer is currently the leading cause of cancer death in the United States and is also the most common type of tumor worldwide. Tobacco smoking is the single most important risk factor for lung cancer. Among the many components of cigarette smoke, polycyclic aromatic hydrocarbons are strongly implicated as causative agents in the development of these cancers (*1*). Benzo[*a*]pyrene, which occurs in amounts of 20 to 40 ng per cigarette, is by far the best studied of these compounds and is one of the most potent mutagens and carcinogens known. The compound requires metabolic activation to become the ultimate carcinogenic metabolite, BPDE [(±)-anti-7β,8α-dihydroxy-9α,10α-epoxy-7,8,9,10-tetrahydrobenzo[a]pyrene], which binds to DNA and forms predominantly covalent (+) trans adducts at the N2 position of guanine (*2*).

About 60% of human lung cancers contain mutations in the *P53* tumor suppressor gene (*3*). The *P53* mutation database (*4*) includes more than 500 entries of sequenced *P53* mutations for lung cancer. There is a large percentage of G to T transversion mutations in these tumors. Such mutations are hallmarks of mutagenesis involving certain types of polycyclic aromatic hydrocarbons, including BPDE (*5*), but they can also be induced by other agents, including oxidative DNA damage (*6*). The distribution of mutations along the *P53* gene in lung cancer is nonrandom but rather is characterized by several mutational hotspots, in particular, at codons 157, 248, and 273 (Fig. 1), which correspond to amino acids within the DNA binding domain of p53. Codon 157 is a mutational hotspot specific for lung cancer and does not occur as a hotspot in any other cancer, but the other two codons are affected in many different tumor types (*3*, *7*). The majority of lung cancer mutations at these three codon positions are G to T transversions (*4*).

To investigate the relation between BPDE adduct formation and *P53* mutations, we mapped the distribution of BPDE adducts along the *P53* gene using a modification of the ligation-mediated polymerase chain reaction (LMPCR) (*8*). HeLa cells were treated with various concentrations of BPDE (*9*), and DNA was isolated and cleaved at the sites of modified bases with the UvrABC nuclease complex from *Escherichia coli* (*10*). UvrABC makes a dual incision 5′ and 3′ to the adducted base, and the 3′ incision occurs specifically at the fourth nucleotide position 3′ to a BPDE adduct (*11*). These break positions can then be visualized by LMPCR in which *P53*-specific oligonucleotide primers were used (*12*, *13*). Figure 2A shows an analysis of the upper (nontranscribed) DNA strand of exon 5. One of the strongest BPDE-derived signals along the exon is seen at codon 157, which is one of the major mutational hotspots in lung cancer. In exon 7, the two guanine positions within the frequently mutated codon 248 are the preferred targets for BPDE adduct formation (Fig. 2B). The same is true for exon 8, where the strongest signal corresponds to a BPDE adduct at the guanine within the mutational hotspot codon 273 (Fig. 2C).

To analyze a cell type that is more representative of the target cell population during lung tissue transformation, we performed similar experiments with normal human bronchial epithelial cells (*14*). The BPDE adduct patterns were generally simi-

M. F. Denissenko and G. P. Pfeifer, Department of Biology, Beckman Research Institute of the City of Hope, Duarte, CA 91010, USA.
A. Pao and M.-s. Tang, M. D. Anderson Cancer Center, University of Texas, Science Park, Smithville, TX 78957, USA.
*To whom correspondence should be addressed.